Toward Teleoperated Needle Steering under Continuous MRI Guidance for Prostate Percutaneous Interventions

Reza Seifabadi[1,2] (RS), Fereshteh Aalamifar[1] (FA), Iulian Iordachita[1] (II), and Gabor Fichtinger[1,2,3] (GF)

[1]Department of Mechanical and Material Engineering, Queen's University, Kingston, ON, Canada.

[2]Laboratory for Computational Sensing and Robotics (LCSR), The Johns Hopkins University, Baltimore, MD.

[3]School of Computing, Queen's University, Kingston, ON, Canada.

Corresponding author: rezaseifabadi@gmail.com, +1 (443) 615-2950.

Type: Original Article

Funding: Research supported by the US National Institute of Health (NIH) under R01CA111288 grant.

Full Paper, 30 pages, 8734 words, 13 Figures, 2 tables.

Abstract

Purpose: To propose a human-operated in-room master-slave bevel-tip needle steering system under continuous MRI guidance for prostate biopsy, in which the patient is kept in the scanner at all times and the process of needle placement is under continuous control of the physician thus making the intervention shorter, less costly, safer, less discomfort to the patient, and more importantly, more accurate by reducing patient motions.

Methods: a 2-DOF MRI-compatible needle steering module (called slave robot) is developed and integrated with an existing 4-DOF transperineal robot, creating a fully actuated 6-DOF (x, y, z, yaw, pitch, and roll) robotic platform for MRI-guided prostate interventions. An MRI-compatible 2-DOF master robot is also developed to enable remote needle steering. An MRI-compatible 2-DOF force/torque sensor was used on the master side. Bevel-tip needle steering is proposed in order to compensate for the targeting error due to needle-tissue interaction.

Results: MRI-compatibility results demonstrated a maximum of 20% loss in Signal to Noise Ratio (SNR). Robot functionality was not influenced by the magnetic field. Targeting error was reduced from 4.2mm to 0.9 mm as the result of bevel-tip needle steering.

Conclusions: The feasibility of teleoperated bevel-tip needle steering using the proposed system was shown in phantom experiment once in a bench-top experiment and once under real-time MRI-guidance.

Keywords: Teleoperation, Continuous MRI guidance, Needle steering.

Introduction:

Prostate cancer is the most common cancer for men in the United States and other western countries. Every year, approximately 1.5 million prostate biopsy procedures are performed in the United States alone [1]. If the prostate specific antigen (PSA) level goes above a certain threshold, patients are advised to undergo a biopsy. If the result is positive, many patients choose low dose brachytherapy (LDR) as it is a minimally invasive treatment method with short recovery time. Brachytherapy requires placing 60-120 radioactive seeds into the prostate using needles so that the radioactive seed irradiate local cancerous lesions. In both biopsy and brachytherapy, needles are manually inserted into the prostate under Transrectal Ultrasound (TRUS) guidance.

Ultrasound guidance is the gold standard method for prostate biopsy and brachytherapy since it is real-time, relatively inexpensive, non-invasive, and easy to use. However, the image quality is rarely sufficient to visualize the cancerous lesions and rather, it shows the prostate boundary. This results in a significant number of false-negative biopsies with lacking detection rate [2]. In brachytherapy, the seeds are barely visible since they are very small and also because their visibility is hindered by the speckle shadow artifact [3].

MRI is a superior imaging modality for its excellent visualization of the prostate lesions, gland, surrounding tissues, and because it is non-invasive. Advances with endorectal and phased array pelvic coils have significantly improved the ability of MRI to visualize prostate tissue [4]. MRI can even provide (near to) real-time imaging.

Since 2000 when the first robot was introduced to assist MRI-guided prostate biopsy and brachytherapy [5], a few robotic systems have been developed [6]. These robots can be categorized into two subtypes: 1) Robots with manual needle insertion; these robots only orient the needle toward the target and the insertion is still performed manually. Similar to manually actuated needle guide devices, these systems require many in-and-out movements of patient during the procedure; 2) Robots with automated needle placement [20]; the major concern

regarding these systems is the exclusion of the clinician from the control loop thus potentially risking patient safety. Given the shortcomings of the previously reported robotic systems, this study seeks to develop a telerobotic system that keeps the patient inside the scanner and takes advantage of the continuous MRI imaging during needle advancement, while keeping the physician in the control loop. Another advantage of the teleoperated approach is that needle insertion may not be performed manually while the patient is inside the bore for two reasons: confined workspace of the MRI scanner and the struggle of the clinician to see the continuous MRI screen while doing manual operation.

Teleoperated needle insertion under MRI guidance has been reported previously; Kokes et al. in [7] reported a 1-Degree of Freedom (DOF) hydraulically actuated needle insertion robot for breast radio frequency ablation under MRI guidance using a commercial haptic device placed outside of the MRI room. Yang et al. in [8] proposed a pneumatically actuated version of the 1-DOF system. Yang et al. in [9] further developed the slave system to a 5-DOF parallel robot which was actuated by pneumatic and piezo electric motors. The master robot was 3-DOF and had similar kinematics to the slave. Tan et al. in [10] developed a 3-DOF MRI-compatible force sensor to monitor the insertion forces for the same robot. Elhawary et al. in [11] reported a 5-DOF robotic system using linear piezo-ceramic motors for transrectal prostate biopsy in 1.5T MRI. This system employed a remotely-driven touch-screen needle insertion console placed inside the scanner room. Tse et al. in [12] reported a 1-DOF haptic device to command the needle insertion driver from outside of the scanner room. Su et al. in [13] reported design requirements of a system for teleoperated needle insertion under continuous MRI for prostate brachytherapy. They proposed using a commercial haptic device as the master robot to command the needle driver from outside the room. Shang et al. in [14] developed a teleoperation system with hybrid pneumatic-piezoelectric actuation for MRI-guided needle insertion with haptic feedback. Piccin et al. in [15] reported development of a bilateral single-DOF non-MRI compatible master device to remotely command the needle driver module of a 5-DOF CT/MRI-guided patient-mounted needle placement robot from outside of the scanner room.

All of the previously reported robot for prostate needle placement under MRI that have been reviewed in Chapter 2 of [45] assume a straight trajectory to reach to the target inside the prostate. In reality, needle bends, prostate moves, and deforms [16]. In this study, we propose using bevel-tip needle steering under continuous MRI-guidance to compensate for these errors.

Other methods for error compensation have been reported in literature: 1) Lagerburg et al. in [17]-[19] proposed a tapping method to decrease the insertion force. Tapping entails small and fast oscillations of needle during insertion resulting in reduction of the force between the needle and tissue. 2) Patriciu et al. in [20] suggested fast needle insertion during MRI-guided transperineal prostate brachytherapy to reduce the error caused by prostate motion. 3) Badaan et al. in [21] reported continuous spinning of the needle as a practical solution to lower insertion force. The main concern for this method is the potential for causing tissue damage as a result of needle spinning; In addition to the mentioned limitations, these methods cannot entirely eliminate the error and rather reduce it to some extent assuming that target does not move during needle insertion. A more efficient approach that may solve this issue is: 4) Flexible needle steering by maneuvering the needle tip inside tissue under image guidance until it reaches the target. Among different methods proposed for steering a flexible needle inside tissue ([22]-[27], [46]-[49]), we use bevel tip needle steering since the design is simple and it could be intuitively controlled by the physician in a teleoperation approach.

The concept of bevel-tip needle steering could be explained as follows: bevel-tip flexible needle is inserted into tissue, it bends due to the asymmetric forces applied to the tip. If the needle is rotated 180 degrees, the needle bends to the opposite direction. Although this idea was initially proposed for obstacle avoidance during percutaneous interventions, we used it for error compensation in this study.

It is worth noting that the asymmetry of the tip could result in error if the needle orientation is not controlled. However, in this study, it is used as a tool to compensate for the error since the needle angle is controlled by the physician. In fact, if the physician observes deviation of the needle from the path to target, he/she could rotate the needle for 180 degree to return the needle tip back toward target. Sometimes, it may be necessary to slightly retract the needle and then rotate the tip for 180 degrees to have further compensation. While this method may not be able to compensate for all sources of error such as the prostate motion, it is a simple and yet an efficient method to minimize the error while still having the physician performing the procedure, which is the major advantage of this proposed approach.

In this study, we present a MRI-compatible robotic platform with full 6-DOF (x, y, z, yaw, pitch, and roll) for prostate needle placement. We present a novel 2-DOF MRI-compatible master robot

and development of controller hardware and software to enable teleoperated needle steering. The design concepts of the master and slave were previously reported in [28]. Also, a 2-DOF MRI-compatible force sensor that utilizes Fiber Bragg Grating (FBG) sensors is employed to address with the non-backdrivability of the master robot that originates from the inherent friction of the piezo actuators. MRI-compatibility results of the system are presented in a 3T MRI scanner. Accuracy of the slave robot in tracking the master robot is performed in an MRI room inside a phantom. The feasibility of bevel-tip needle steering in phantom is demonstrated under continuous MRI-guidance.

Materials and Methods:

Fig. 1 exhibits the entire system architecture. On the right side, the previously developed base robot system components are shown as black rectangles [29]-[32] while on the left side, teleoperated needle steering system components developed in this study are shown in red.

Base robot system architecture and components

The base robot system consists of a 4-DOF parallel manipulator hereafter referred to as the base robot, base robot controller, planning and navigation workstation, power box A, MRI host workstation, local network A, and computer A (Fig. 1). The base robot and its controller are placed inside the MRI room while the rest are placed in control room. Fig. 2 shows the base robot. The robot was designed for manual needle insertion. Four pneumatic actuators are used to move the four sliders. The movement of the 4 sliders enables translations and rotations of the needle in the x, y and Rx, Ry directions, respectively.

Fig. 1.

Fig. 2.

The base robot controller consists of a Linux PC, piezo electric valves, and a media converter all placed into a radio frequency shielded cage. The controller uses medical air in a hospital to run the base robot. The power supply is placed in control room and is plugged to the controller through a patch panel (which is a RF shielded panel in MRI rooms). Registration of the robot coordinate system to MRI coordinate system is done by Z-frame [29]. Z-frame is a cube with three Z patterns (filled with gadolinium) on three faces of that cube as described in [29]. The monitor in control room displays the air pressure and the encoders' positions. Details of the base robot kinematics and system architecture can be found in [30], and [32].

Teleoperated needle steering system architecture and components

The teleoperated needle steering system proposed in this study consists of: 1) a 2-DOF needle steering slave robot which is integrated with the base robot yielding a 6-DOF manipulator, 2) an MRI-compatible 2-DOF master robot, 3) master-slave controller, 4) two MRI-compatible monitors for continuous MR image and for graphical user interface (GUI), 5) an FBG

interrogator for wavelength shift measurement (used in force measurement), 6) a power supply box B, 7) a local network B, and 8) the computer B for force calculations, previewing GUI, and sending and receiving data to master-slave controller. Master-slave controller is placed next to the patch panel. The master robot and the monitor are placed next to the patient.

Data between the master-slave controller and computer B is transmitted thorough optical fiber cable. In fact, inside master-slave controller box and power box B, there are two identical media convertors that exchange data into optic signals and vice versa, meaning the data transmission between the MRI room and the control room is in optical form with no interference with MRI. The local network in the control room aims to connect the FBG interrogator and master-slave controller to the computer B. The power cord is connected to master-slave controller through the patch panel to minimize Electromagnetic Interference (EMI).

The proposed biopsy procedure using this system is as follows:

1) The patient is placed on MRI table in lithotomy position.
2) A Z-pattern fiducial frame is placed on a predefined position on the patient board and registration is done.
3) The Z-frame is removed and the base robot is placed between the patients legs in a defined position on the patient board.
4) The patient is moved into the scanner and images are acquired. The prostate images are sent from the MRI host workstation to 3D Slicer (planning and navigation workstation).
5) In 3D Slicer, a suspicious target and needle path is specified by the physician. Then, this information is sent to the base robot controller.
6) The robot controller moves the robot such that the needle is aligned toward the target. Now, the needle is ready to be inserted.
7) The physician holds the needle mimicking stylet of the master robot as if he/she is inserting and/or rotating the bevel-tip needle at the slave side.
8) The slave translates (rotates) the needle with a velocity equal to the master's translation (rotation). The physician observes needle advancement under continuous MRI and monitors the accuracy of tracking and the depth (or the needle rotation) on the GUI.

9) If the needle is deviating from the target, physician retracts the needle a little bit and rotates the needle 180 degrees. Then, the insertion is resumed until reaching the target.
10) Next, the patient is removed and the sample tissue is taken out. These steps are repeated until all targets are sampled. The flowchart in Fig. 3 shows the workflow.

Fig. 3.

A. Slave Robot

The slave robot generates a combination of linear and rotary motions for the bevel-tip needle so that needle steering is enabled (Fig. 4). Figure 5 shows that the slave robot is integrated with the base robot yielding a 6-DOF fully actuated robotic platform for MRI-guided prostate interventions. We used non-magnetic piezo motors (PiezoLEG Uppsala, Sweden) with PDA 3.1 drivers (50 Nmm, 5.5 RPM). Some advantages of this motor are high accuracy, small size, and offering an easy to control driver (+/-10V standard) and negligible noise on MR image [33].

It is preferred to design the slave robot to be non-backdrivable so that in the case of power failure, the needle holds its own position. This is naturally provided by the inherent friction of the piezo motor.

Linear stage: The linear motion is provided by a house-made belt drive which consists of a timing belt, two small brass timing belt pulleys, two aluminum anodized shafts, and a slider (Fig. 4). Belt drive was chosen due to its smaller friction and minimum backlash. The slider carrying needle rotation stage and needle holder slides on two aluminum shafts and is fixed to the timing belt thus moving with the timing belt. Power is provided by piezo motor M1 and is transmitted by another timing belt and a pair of pulleys (in Fig. 4 only one pulley is visible, B). The gear

ratio between D and E was chosen to be 4:3 so that a speed of 2.5 mm/sec is attained. The travel is 140 mm, enough to reach targets deep into the prostate (usually, targets are 70-110 mm deep). Optical encoder E1 (EP8 OEM, US Digital, Vancouver, WA) is placed concentric to motor M1 shaft in order to measure the linear displacement of the needle. All other parts are made of plastic (either 3D printing or cast acrylic) or brass.

Fig. 4.

Fig. 5.

Rotary stage: The rotary motion is generated by a second motor M2. The power is transmitted to the needle holder using two pulleys: F and G (Fig. 4). The gear ratio between F, G is 2:1 to increase the speed of rotation. The needle is held by a hollow pin-vice made of brass. The needle is loaded from behind for convenience. Optical encoder E2 is used to measure needle orientation (EP8 OEM, US Digital, Vancouver, WA).

Typically, an 18G needle (∅ = 1.3 mm) is used for prostate biopsy and brachytherapy. In this study however, we used an MRI-compatible 20G × 15 cm bevel-tip biopsy needle (Cook Inc, IN, USA) to achieve increased flexibility so that we can compensate for the errors caused by the needle-tissue interaction.

B. Master Robot

Similar to the slave robot, the master has 2-DOF: needle insertion and needle rotation. Figure 6 shows the prototype of the proposed master robot. The physician grasps a small diameter cylinder (called stylus) that mimics the needle and manipulates it as if he or she is performing real needle steering.

Fig. 6.

Linear stage: In this study, a Peaucellier-Lipkin mechanism (Fig. 6) was chosen due to the following advantages: 1) there is no sliding joint in this mechanism meaning that friction is minimal; 2) its effector (point P) in theory travels a perfect line throughout the workspace; 3) no counter balancing is necessary since the mechanism can be configured horizontally; The actuator is placed stationary at joint B. As motor M1 and its encoder rotates, the stylus travels in an accurate straight line. Detail of the design, kinematic analysis, dynamic analysis, and link sizes of the mechanism was discussed in [28].

Rotary stage: Motor M2 and its encoder are designed to be fixed to the base. The bar mimicking needle is selected to be hexagonal (made of brass) and passes through a small shaft with a hexagonal hole in the center. The shaft is press-fit at the center of pulley 4. The shaft (made of brass with a wire EDM) allows needle to translate but constraints it from rotation. Pulley 4 is connected to pulley 3 which is concentric to the motor M2 via a timing belt. As a result, the rotation of the stylus (the hexagonal bar) is transmitted to the rotary motor which is fixed to the base. In this way, the motor and encoder of the rotary stage remain stationary in order to minimize the inertia of the moving parts.

The box, linkages, and motor supports are made from cast acrylic sheet (McMaster.com). All other parts are made from non-ferromagnetic metals (brass and aluminum) and plastic. Plastic

and brass bearings were used for all rotary joints in order to minimize friction. The motors are piezo motors, similar to the slave robot.

C. Controller

Controller hardware: Figure 7 shows the controller hardware and inside components. The controller hardware consists of four PDA 3.1 piezo motor drivers (PDA 3.1, PiezoMotor, Upsala, Sweden), a 4-axis DMC-2143 Ethernet motion controller (Galil Motion Control, Rocklin, CA, USA), a media converter (B&B Electronics Mfg. Co., Ottawa, IL, USA), and a 5A, 24 to 12 DC-DC converter (Linear power Inc., Pearl, MS, USA). All of these parts are placed inside an aluminum enclosure (Faraday cage) to minimize EMI. Ventilation is considered on top of the case. The encoders and motors are plugged using 9-pin connectors making the system installation quick and easy. Also, the power and optical cable are plugged into the box. The motion controller communicates with the laptop in the control room through the optical cable. On computer B in Fig. 1, GalilTools is used to command the controller. A 24 V DC power supply is used to run the controller, drivers, and media converter. Since the drivers work with a different voltage (12V) from Galil controller and media converter (24V), a DC-DC convertor is used.

Fig. 7. Left: Master-slave controller box intside view, Right: Power supply box.

Figure 7-Right shows the power supply box. It consists of a 24V power supply and a media converter. Media converter of power supply box gets the command from computer B through Ethernet cable and converts it to optical data. The optical data are transmitted through the optic cable to MRI room. At media converter inside the controller box, the optic data are converted back to electrical data and go to controller through an Ethernet cable. The opposite of this process is performed when Galil controller sends data to the computer B.

Controller algorithm: The controller aims to maintain position tracking between the master and the slave robots. Since translation and rotation motions are independent, two separate controllers

were considered, one for translation and another for rotation. One big challenge during controller design was the fact that master robots are non-backdrivable as a result of the inherent friction of piezo motors. While it is an advantage for the slave (self-brake in case of power failure), it is a drawback for the master since it is not possible to initiate the movement. We developed an MRI-compatible force/torque sensor [34] as depicted in Fig. 6, primarily for measuring the force applied to the needle which we want to feedback to the physician's hand through the master robot. However here, we used it to solve non-backdrivability of the master as follows; when the operator applies force or torque to the stylus, the stylus translates/rotates with a speed proportional to the amount of torque/force applied by the physician's hand. In fact, the controller and physician share the control of the master robot (referred to as cooperative control [35]). Figure 8 shows this concept. Force F_h (or τ_h) is multiplied to a constant k_f (k_τ). The output is the desired velocity (angular velocity). A PID controller ensures that the angular velocity of the master translational motor (rotational motor) will track this desired velocity. After the master's movement is initiated, another PID controller guarantees that the slave's position follows the master's position. Table I shows the controller gains and parameters. KD, KP, and KI are differential, proportional, and integral gains respectively. The gains were found by trial and error such that while the system remains stable at all time, the instantaneous error between the master and slave (i.e. $x_m - x_s$, $\theta_m - \theta_s$) is minimized both in free space motion and while inserting the needle into the phantom.

TABLE I.

Fig. 8.

Controller software: The controller code was written in G-language (a language developed by the Galil Co. for their controllers) and was compiled on the Galil controller using GalilTools, which is the user interface for Galil motion controllers. The input signals to the motion controller

are Fh, τh, as well as position information coming from encoders, i.e. x_m, x_s, θ_m and θ_s. The encoders are directly connected to the controller while the force and torque information is received from the MATLAB code running on computer B in control room. G-codes can be accessed within MATLAB using command *g.command (.)* making communication between the GalilTools and MATLAB possible [36]. This communication is bilateral, i.e. a MATLAB code sends force and torque to the controller and controller sends the position information of the robots to a GUI which is written in MATLAB.

D. MRI-Compatible force sensor

An MRI-compatible sensor which is capable of measuring axial force and torque is required on the master side in order to address the non-backdrivability of the master robot using the cooperative control as explained before. Since an MRI-compatible force sensor is not available commercially, such a sensor was developed using a Fiber Bragg Grating as strain gauges. The force sensor can measure axial forces in the range ± 20 N and axial torques in the range of ± 200Nmm with 0.1 N and 1 Nmm resolution, respectively. The sensor is a cylinder of diameter = 15mm and height = 20mm. The sensor accounts for environment temperature changes. Four FBGs are used to measure the axial force and torque. Optical fibers with 2 mm long FBGs, wavelength 1545nm, were purchased off the shelf from Technica SA (Beijing, China). A FBG interrogator is a device that generates light and measures the wavelength shift of the reflection. In this study, we used a 4 channel Micron Optics sm130 (Atlanta, GA, USA), with sampling rate of 2 KHz. The spectrum ranges from 1525 nm to1565 nm. Each channel handles one fiber.

In order to use the sensor, we passed the fibers through the patch panel and plugged them into the FBG interrogator which is placed in the control room. Since the sensor is made of non-magnetic material (phosphor-bronze, and plastic for casing) and it only uses light, it is MRI-compatible by nature. The FBG interrogator sends the wavelength shifts with some other information to the computer B via an Ethernet port in real-time. In the MATLAB code, the wavelength shifts are extracted from the raw data and calibration coefficients (found after calibration procedure) are applied thus determining the axial force and torque. The axial force and torque measurements are then sent to the Galil controller in MRI room. Detailed discussion

of the force sensor is provided in [34]. A video demonstrates the performance of this force sensor in comparison with a commercial non-MRI compatible force sensor [38].

Experiments and Results

A. MRI-compatibility

MRI-compatibility can be defined as follows: 1) the device does not develop a risk to patient and clinicians' safety. This can either be a flying object due to the magnetic force or RF heating caused by metal parts. 2) The image quality deterioration as a result of putting the system in the MRI room is insignificant. 3) The device can properly function inside the MRI room while the scanner is operating. In the following, MRI-compatibility from these perspectives is evaluated.

MRI safety: In this study, the master and the slave robots were made from nonmagnetic materials with minimal metal parts to avoid Eddy current and therefore, RF heating. The controller components were placed into an aluminum enclosure and the controller box was placed next to the patch panel inside MRI room. The only object that touches the patient is the needle, meaning the risk of RF heating is minimized. During the MR imaging, no temperature change was observed by touching the needle.

Image quality: Ferromagnetic materials (even tiny set-screws) were eliminated in order to minimize EMI. The use of other metals was minimized to avoid Eddy currents that results in RF heating and EMI. Cables of the piezo motors and encoders that have the most significant contribution to EMI were properly shielded and grounded. Since the encoders in this study are differential, we used shielded twisted-pair cables (US Digital, part No. CA-MIC6-SH-NC) in order to minimize this noise to the maximum extent possible. During the experiment, we observed that the encoders of the slave drop SNR up to 35% resulted from the interference of the MRI magnetic field with the unshielded encoder's PCB circuit. We fixed this issue by wrapping the encoder enclosures (black objects in Fig. 4) using aluminum foil. The controller components were placed into an aluminum cage, and the box was placed next to the patch panel. Also, we used motors and drivers.

With these considerations, we conducted an SNR test using a 3T GE Discovery MR750 (General Electric Healthcare, Waukesha, WI, USA). A cylindrical MRI phantom (∅ = 110 mm × 230) mm was placed in the iso center and the robot placed so that the base robot front is 2 cm from the cylinder (similar to the relative position of the robot and patient). A round flex coil similar to those often used in prostate imaging was used. The phantom was imaged using three standard prostate imaging protocols:

1- T1 FGE: T1 weighted fast field gradient echo for diagnostic imaging;

2- T2 FSE: T2 weighted fast spin echo for diagnostic imaging;

3- TFE (FSPGR): "continuous" turbo field gradient echo.

Imaging parameters are provided in Table II.

The following imaging series were taken: 1) phantom only (baseline); 2) System in (i.e. the master next to the scanner, the 6-DOF robot inside the bore, and controller inside the room next to the patch panel), but power off; 3) The power was turned on, but the cables of the motors and encoders remained unplugged; 4) The cables of the master robot we plugged only (2 for motors and 2 for encoders); 5) The cables of the slave robot we plugged only; 6) All cables were plugged; 7) The master and slave moved at the same time (teleoperation was enabled). We used NEMA standard - method 4 to measure SNR [38]. This standard defines SNR as the mean pixel charge in a square in the center of the image (signal) divided by the mean value of the Raleigh distribution of the noise region (corner of the image background where only noise exists). The results were normalized by the value of the baseline image. Fig. 9 shows the results.

TABLE II.

Fig. 9.

From Fig. 9, the following observations can be made: 1) the system does not contribute any significant noise before moving (less than 10% SNR loss in all scenarios). 2) The SNR loss when the robots are moving is almost 30 percent. Figure 10 visually compares different imaging sequences for baseline with the system moving. Since teleoperated needle seeing is performed with a human operator, we think this SNR loss is acceptable.

Fig. 10.

B. System functionality

The functionality of the teleoperated needle steering system in MRI room was evaluated while the scanner was running. The 6-DOF robot was placed inside the bore, the master was placed next to the scanner and the system was powered on. The purpose of the following experiments is to demonstrate that the functionality of the system i.e. position tracking is not affected while MRI is running. The folowing experiment was conducted:

Needle insertion into prostate phantom: The purpose of this experiment was to evaluate the tracking accuracy when the needle is inserted into the tissue. First, the master robot was moved forward with an arbitrary speed. We were interested if the slave could follow the master both accurately and quickly with small time delay. Next, the mater stylus was rotated with an arbitrary speed clockwise. Again, it was expected that the slave could follow the master accurately with tiny time delay. Figure 11 shows the results.

Fig. 11.

From Fig. 11, it can be observed that the slave robot can track the master robot with accuracy better than 0.5 mm in translation and 5 degrees in rotation during needle steering. The steady state error however was zero. These results demonstrated that MRI has no negative impact on the functionality of the system. A video demonstrating system's functionality in MRI room is provided in [39].

C. Feasibility of teleoperated needle steering in phantom trial on bench-top setup

In the previous section, we proved that the slave can follow the master with sufficient accuracy. Theoretically, needle insertion and rotation plus continuous image feedback enables physician to perform bevel-tip needle steering. However, a more realistic experiment was sought to demonstrate the feasibility of needle steering using the proposed master-slave system and its capability in error compensation.

The setup was almost the same as what was shown for the real experiment in MRI room with the difference of having video feedback of a semi transparent soft plastic phantom instead of the continuous MRI image. It was assumed that the base robot has already oriented the needle toward the target (the accuracy of the base robot in needle orientation was reported previously in [16]). A semi transparent phantom was made using tissue mimicking soft plastic materials with the ratio of 5 to 1 (softener to hardener). The phantom box was created using a laser cutter (70 × 70 × 20 mm- dimensionally, this is different from the phantom used in the next section). On each two opposing faces of the box, 5 holes were made with the laser cutter with 0.1 mm accuracy.

Each hole on one side was therefore precisely aligned with another hole on the opposite side. A video demonstrates the performance of the system showed in is provided in [40].

The experiment was performed as follows using two users: for each target (5 targets in total), once the user inserted the needle without any steering until reaching the opposite wall of the phantom and once with steering. Steering here entailed to insert the needle approximately half-way through, rotate the bevel-tip 20G needle for 180 degrees and then, continue the insertion until reaching the opposite side of the phantom. Figure 12 compares the errors. Since the needle leaves a path inside the phantom after the first insertion, user 2 used another 5 holes which were made on the other two opposing faces of the phantom.

The results show that the error has significantly reduced as the result of this simple steering technique. Although the error numbers may not be quite representative of the human tissue, the relative reduction in error may still hold in the human tissue. A video demonstrating this difference is provided in [41].

Fig. 12.

D. Feasibility of teleoperated needle steering under continuous MRI guidance

The feasibility of teleoperated needle steering under continuous MRI guidance was studied in a phantom experiment. FSPGR imaging with 2 slices per second was utilized for continuous visual feedback. Figure 13 shows the experimental setup. It was assumed that the base robot has already oriented the needle toward the target (the accuracy of the base robot in needle orientation was reported previously in [16] and [31]). A phantom was made using tissue mimicking soft

plastic materials (M-F Manufacturing, Inc., Ft. Worth, TX, USA). The phantom box was created using a laser cutter (90 × 90 × 50 mm). On the two opposing faces of the box, 8 holes were made with the laser cutter. Each hole on one side was therefore precisely aligned with another hole on the opposite side.

Fig. 13.

The phantom was placed in front of the 6-DOF robot. The needle was inserted partially into a hole before starting the experiment. Two visible markers (donut-shape) were placed concentric to those two holes made in the opposite walls of the phantom so that the entry point and the target are visible in the MR image. Therefore, the goal was to reach the other visible marker which was at 80 mm distance from the entry point. The operator held the master robot and inserted the needle under continuous MRI.

Figure 14 shows the continuous MR image in which needle-tip artifact is visible as the needle was gradually inserted. The imaging plane was set so that it can capture the needle shaft and the visible markers (in a sagittal plane). Since the artifact is a few millimeter thick, it cannot precisely represent the needle tip location (to solve this issue, we proposed a method of 3D shape needle shape tracking using FBG sensors with sub-millimeter accuracy [42]). Nevertheless, it was quite straightforward to follow the needle-tip in continuous MR image. When the needle reached almost half-way through, the operator rotated the needle 180 degrees and continued insertion. The needle was retracted after reaching the opposite wall of the phantom. This preliminary experiment showed that teleoperated needle steering under continuous MRI guidance could be performed with the proposed system and methodology. Figure 14 shows the needle tip at 4 intervals through insertion. At time step (c), the operator rotated the needle 180 degrees.

Fig. 14.

Discussions, Conclusions, and Future Work

In order to have continuous human supervision in the loop and to decrease the number of patient removals from the scanner, this study presented a master-slave approach for robot-assisted MRI-guided prostate needle placement. Teleoperated needle steering under continuous MRI guidance was proposed and enabled in order to compensate for errors introduced during needle insertion. For this purpose, a 2-DOF MRI-compatible needle steering module was developed and integrated with a 4-DOF transperineal robot, yielding a fully actuated 6-DOF robotic platform for prostate needle placement. A novel MRI-compatible 2-DOF haptic device was also developed to enable teleoperated needle steering while the physician is standing inside the MRI room. A house-made 2-DOF force sensor was used to address the inherent friction of the piezo motors using a cooperative control architecture. Controller hardware and software were developed and implemented to perform this task. MRI-compatibility results showed small SNR degradation of the system. Targeting error reduced from 4.2 mm to 0.9 mm due to the bevel-tip needle steering in a benchtop phantom study. Experiments in the MRI room proved that the

system functionality is not affected by MRI. Also, the feasibility of teleoperated needle steering under continuous MRI was demonstrated in a phantom.

In this study, a static phantom was used with small target motion due to tissue deflection. In order to have a more realistic scenario, capability of needle steering should be experimented in a more realistic phantom such as one reported in [43].

Since the surgical needle leaves a large artifact on continuous MR image, it is hard to track needle tip and therefore, compensate for the error. In addition, continuous MRI imaging involves some latency (typically, 500 msec). An alternative approach with higher accuracy and bandwidth in capturing the 3D shape of the needle is to track the needle using a Fiber Bragg Grating sensor [42].

Also, it is desired to replicate a similar force sensor and place it behind the needle on the slave side so that bilateral teleoperation with haptic feedback can be achieved during needle steering. However, this will introduce a new challenge: the 0.5 sec latency of the MR imaging may impact the system stability and transparency. This means more sophisticated controller architecture is necessary to make the system stable even in the presence of this time delay in visual feedback. This is not an issue and is addressable. However, the transparency of the system will be somehow compromised because the operator is updated about the force at the slave side every 0.5 sec. This limitation cannot be addressed unless continuous MR imaging is offered. Currently, continuous MR imaging with up to 33 msec latency has been achieved in research scanners. Therefore, this issue seems to be resolved in the near future [44].

This system will be modified for patient trials in near future after reconsidering sterilization and safety issues.

Acknowledgements

The authors would like to thank Professor Louis Whitcomb from Department of Mechanical Engineering, Johns Hopkins University, for his support. Gabor Fichtinger was supported as a Cancer Care Ontario Research Chair. The authors also sincerely thank Dr. Kevin Cleary and Dr.

Stanley Fricke from Children's National Health System in Washington DC for their support during MRI experiment.

References

[1] R. Siegel, D. Naishadham and A. Jemal, "Cancer statistics, 2012," CA: A Cancer Journal for Clinicians, 2012.

[2] C. Tempany, S. Straus, N. Hata and S. Haker, "MR‐guided prostate interventions," Journal of Magnetic Resonance Imaging, vol. 27, pp. 356-367, 2008.

[3] B. H. Han, K. Wallner, G. Merrick, W. Butler, S. Sutlief and J. Sylvester, "Prostate brachytherapy seed identification on post-implant TRUS images," Med. Phys., vol. 30, pp. 898, 2003.

[4] A. Krieger. "Advances in magnetic resonance image guided robotic intervention". Ph.D. dissertation, Dept. Mech. Eng., Johns Hopkins Univ., Baltimore, MD, 2008.

[5] K. Chinzei, N. Hata, F. Jolesz and R. Kikinis, "Surgical assist robot for the active navigation in the intraoperative MRI: Hardware design issues," in Intelligent Robots and Systems, 2000.(IROS 2000). Proceedings. 2000 IEEE/RSJ International Conference on, 2000, pp. 727-732.

[6] K. J. Macura and D. Stoianovici, "Advancements in Magnetic Resonance–Guided Robotic Interventions in the Prostate," Topics in Magnetic Resonance Imaging: TMRI, vol. 19, pp. 297, 2008.

[7] R. Kokes, K. Lister, R. Gullapalli, B. Zhang, A. MacMillan, H. Richard and J. P. Desai, "Towards a teleoperated needle driver robot with haptic feedback for RFA of breast tumors under continuous MRI," Med. Image Anal., vol. 13, pp. 445-455, 2009.

[8] B. Yang, U. X. Tan, A. B. McMillan, R. Gullapalli and J. P. Desai, "Design and control of a 1-DOF MRI-compatible pneumatically actuated robot with long transmission lines," Mechatronics, IEEE/ASME Transactions on, vol. 16, pp. 1040-1048, 2011.

[9] B. Yang, S. Roys, U. Tan, M. Philip, H. Richard, R. P. Gullapalli, and J. P. Desai. "Design, development, and evaluation of a master-slave surgical system for breast biopsy under continuous MRI." The International Journal of Robotics Research (2013): 0278364913500365.

[10] U. X. Tan, B. Yang, R. Gullapalli and J. P. Desai, "Triaxial MRI-compatible fiber-optic force sensor," Robotics, IEEE Transactions on, vol. 27, pp. 65-74, 2011.

[11] H. Elhawary, Z. Tse, M. Rea, A. Zivanovic, B. Davies, C. Besant, N. de Souza, D. McRobbie, I. Young and M. Lamperth, "Robotic system for transrectal biopsy of the prostate: Real-time guidance under MRI," Engineering in Medicine and Biology Magazine, IEEE, vol. 29, pp. 78-86, 2010.

[12] Z. Tse, H. Elhawary, M. Rea, I. Young, B. Davis and M. Lamperth, "A haptic unit designed for magnetic-resonance-guided biopsy," Proc. Inst. Mech. Eng. Part H J. Eng. Med., vol. 223, pp. 159-172, 2009.

[13] H. Su, W. Shang, G. A. Cole, K. Harrington and G. S. Fischer, "Haptic system design for MRI-guided needle based prostate brachytherapy," in Haptics Symposium, 2010 IEEE, 2010, pp. 483-488

[14] W. Shang, H. Su, G. Li, and G. S. Fischer. "Teleoperation system with hybrid pneumatic-piezoelectric actuation for MRI-guided needle insertion with haptic feedback." In Intelligent Robots and Systems (IROS), 2013 IEEE/RSJ International Conference on, pp. 4092-4098. IEEE, 2013.

[15] O. Piccin, L. Barbé, B. Bayle, M. De Mathelin and A. Gangi, "A force feedback teleoperated needle insertion device for percutaneous procedures," The International Journal of Robotics Research, vol. 28, pp. 1154-1168, 2009.

[16] R. Seifabadi, N. B. J. Cho, S. E. Song, J. Tokuda, N. Hata, C. M. Tempany, G. Fichtinger and I. Iordachita, "Accuracy study of a robotic system for MRI ‐ guided prostate needle placement," The International Journal of Medical Robotics and Computer Assisted Surgery, 2012.

[17] V. Lagerburg, M. A. Moerland, J. J. Lagendijk and J. J. Battermann, "Measurement of prostate rotation during insertion of needles for brachytherapy," Radiotherapy and Oncology, vol. 77, pp. 318-323, 2005.

[18] V. Lagerburg, M. A. Moerland, M. van Vulpen and J. J. W. Lagendijk, "A new robotic needle insertion method to minimize attendant prostate motion," Radiotherapy and Oncology, vol. 80, pp. 73-77, 2006.

[19] V. Lagerburg, M. Moerland, M. Konings, R. Van de Vosse, J. Lagendijk and J. Battermann, "Development of a tapping device: a new needle insertion method for prostate brachytherapy," Phys. Med. Biol., vol. 51, pp. 891, 2006.

[20] A. Patriciu, D. Petrisor, M. Muntener, D. Mazilu, M. Schär and D. Stoianovici, "Automatic brachytherapy seed placement under MRI guidance," Biomedical Engineering, IEEE Transactions on, vol. 54, pp. 1499, 2007.

[21] S. Badaan, D. Petrisor, C. Kim, P. Mozer, D. Mazilu, L. Gruionu, A. Patriciu, K. Cleary and D. Stoianovici, "Does needle rotation improve lesion targeting?" The International Journal of Medical Robotics and Computer Assisted Surgery, vol. 7, pp. 138-147, 2011.

[22] S. DiMaio and S. Salcudean, "Needle steering and model-based trajectory planning," Medical Image Computing and Computer-Assisted Intervention-MICCAI 2003, pp. 33-40, 2003.

[23] P. E. Dupont, J. Lock, B. Itkowitz and E. Butler, "Design and control of concentric-tube robots," Robotics, IEEE Transactions on, vol. 26, pp. 209-225, 2010.

[24] D. C. Rucker, B. A. Jones and R. J. Webster, "A geometrically exact model for externally loaded concentric-tube continuum robots," Robotics, IEEE Transactions on, vol. 26, pp. 769-780, 2010.

[25] H. Su, D. C. Cardona, W. Shang, A. Camilo, G. A. Cole, D. C. Rucker, R. Webster and G. S. Fischer, "A MRI-guided concentric tube continuum robot with piezoelectric actuation: A feasibility study," in Robotics and Automation (ICRA), 2012 IEEE International Conference on, 2012, pp. 1939-1945.

[26] C.Walsh, “Image-guided robots for dot-matrix ablastion,” PhD dissertation, Dept. Mech. Eng., Massachusetts Institute of technology (MIT), Chapter 5, 2010.

[27] R. J. Webster III, J. S. Kim, N. J. Cowan, G. S. Chirikjian and A. M. Okamura, "Nonholonomic modeling of needle steering," The International Journal of Robotics Research, vol. 25, pp. 509-525, 2006.

[28] R. Seifabadi, I. Iordachita and G. Fichtinger, "Design of a teleoperated needle steering system for MRI-guided prostate interventions," in Biomedical Robotics and Biomechatronics (BioRob), 2012 4th IEEE RAS & EMBS International Conference on, 2012, pp. 793-798.

[29] G. S. Fischer, I. Iordachita, C. Csoma, J. Tokuda, S. P. DiMaio, C. M. Tempany, N. Hata and G. Fichtinger, "MRI-compatible pneumatic robot for transperineal prostate needle placement," Mechatronics, IEEE/ASME Transactions on, vol. 13, pp. 295-305, 2008

[30] S. E. Song, N. B. Cho, G. Fischer, N. Hata, C. Tempany, G. Fichtinger and I. Iordachita, "Development of a pneumatic robot for MRI-guided transperineal prostate biopsy and brachytherapy: New approaches," in Robotics and Automation (ICRA), 2010 IEEE International Conference on, 2010, pp. 2580-2585.

[31] J. Tokuda, S.E. Song, G.S. Fischer, I. Iordachita, R. Seifabadi, N.B. Cho, K. Tuncali, G. Fichtinger, C.M. Tempany, and N. Hata, “Preclinical evaluation of an MRI-compatible pneumatic robot for angulated needle placement in transperineal prostate interventions,”

International Journal Of Computer Assisted Radiology And Surgery (IJCARS), DOI: 10.1007/s11548-012-0750-1, 2012.

[32] R. Seifabadi, S. E. Song, A. Krieger, N. B. Cho, J. Tokuda, G. Fichtinger and I. Iordachita, "Robotic system for MRI-guided prostate biopsy: feasibility of teleoperated needle insertion and ex vivo phantom study," International Journal of Computer Assisted Radiology and Surgery, vol. 7, pp. 181-190, 2012.

[33] H. Elhawary, Z. Tse, M. Rea, A. Zivanovic, B. Davies, C. Besant, N. de Souza, D. McRobbie, I. Young and M. Lamperth, "Robotic system for transrectal biopsy of the prostate: Real-time guidance under MRI," Engineering in Medicine and Biology Magazine, IEEE, vol. 29, pp. 78-86, 2010.

[34] R. Monfaredi, R. Seifabadi, G. Fichtinger, and I. Iordachita, “Design of a decoupled MRI-compatible force sensor for robot-assisted prostate interventions,” In SPIE Medical Imaging, pp. 867118-867118, 2013.

[35] R.H. Taylor, P. Jensen, L.L.Whitcomb, A. Barnes, R. Kumar, D. Stoianovici, P. Gupta, Z. Wang, E. de Juan, and L. Kavoussi, “Steady-hand robotic system for microsurgical augmentation, “The International Journal of Robotics Research, 18(12), pp. 1201-1210. 1999.

[36] Application Note #4424, Programming MATLAB ® with Galil controllers. www.galilmc.com/support/appnotes/software/note4424.pdf

[37] NEMA Standards Publication MS 1-2008: Determination of Signal-to-Noise Ratio (SNR) in Diagnostic Magnetic Resonance Imaging. National Electrical Manufacturers Association, www.nema.org.

[38] Video of the MRI-compatible force/torque sensor https://www.youtube.com/watch?v=QSHHaWpshZA

[39] Video of the teleoperated needle steering system in a 3T MRI: https://www.youtube.com/watch?v=WVL583Z1RZQ

[40] Video of the teleoperated needle steering system during a benchtop experiment: https://www.youtube.com/watch?v=uNVzIPBexps

[41] Video of the effectiveness of needle steering in reducing error in needle placement: https://www.youtube.com/watch?v=cR9-FfoDKsY

[42] R. Seifabadi, E. E. Gomez, F. Aalamifar, G. Fichtinger, and I. Iordachita. "Real-time tracking of a bevel-tip needle with varying insertion depth: Toward teleoperated MRI-guided needle steering." In Intelligent Robots and Systems (IROS), 2013 IEEE/RSJ International Conference on, pp. 469-476. IEEE, 2013.

[43] N. Hungr, M. Baumann, J. Long and J. Troccaz, "A 3-D Ultrasound Robotic Prostate Brachytherapy System With Prostate Motion Tracking," Robotics, IEEE Transaction on, 2012.

[44] S. Zhang, M. Uecker, D. Voit, K. D. Merboldt, and J. Frahm “Technical notes Real-time cardiovascular magnetic resonance at high temporal resolution: radial FLASH with nonlinear inverse reconstruction,” Journal of Cardiovascular Magnetic Resonance, Open access, pp. 12-39, 2010.

[45] R. Seifabadi, PhD thesis, Mechanical and Material Engineering Department, Queen’s University, Canada, May 2013.

[46] R. Alterovitz, M. Branicky, and K. Goldberg. Motion planning under uncertainty for image-guided medical needle steering. The International Journal of Robotics Research, 27(11–12): pp. 1361–1374, 2008.

[47] K. G. Yan, T. Podder, Y. Yu, T.I. Liu, C.W.S. Cheng, and W.S. Ng, Flexible needle–tissue interaction modeling with depth-varying mean parameter: preliminary study. IEEE Transactions on Biomedical Engineering, vol. 56(2):pp. 255–262, 2009.

[48] S. Onogi, Y. Nakajima, T. Koyama, Y. Tamura, E. Kobayashi, I. Sakuma, N. Sugano and K. Yonenobu, "Robotic vertebral puncture system for percutaneous vertebroplasty," J. Med. Biol. Eng., vol. 33: pp. 491-496, 2013.

[49] S. Jiang, P. Li, Y. Yu, J. Liu, Z. Yang, Experimental study of needle-tissue interaction forces: Effect of needle geometries, insertion methods and tissue characteristics, Journal of biomechanics, vol. 47(13), pp. 3344-335, 2014.

TABLE I. CONTROLLER PARAMETERS

	KD	**KP**	**KI**	k_f **(SI)**	k_τ **(SI)**
Master linear	100	277	12	4.1e-3	2e-3
Slave linear	277	800	4	-	-
Master rotary	256	584	0.5	-	-
Slave rotary	250	500	4	-	-

TABLE II. IMAGING PARAMETERS USED FOR SNR TESTS.

Protocol	T1 FGE	T2 FSE	FSPGR
Thickness	3 mm	3 mm	3 mm
FOV	240 mm	240 mm	240 mm
#Slices	10	10	10
TE	2.2 ms	88 ms	4.2 ms
TR	225 ms	3000 ms	26 ms
Flip Angle	75 deg	90 deg	70 deg
NEX	1	1	1
Bandwidth	977 Hz/pixel	244 Hz/pixel	244 Hz/pixel

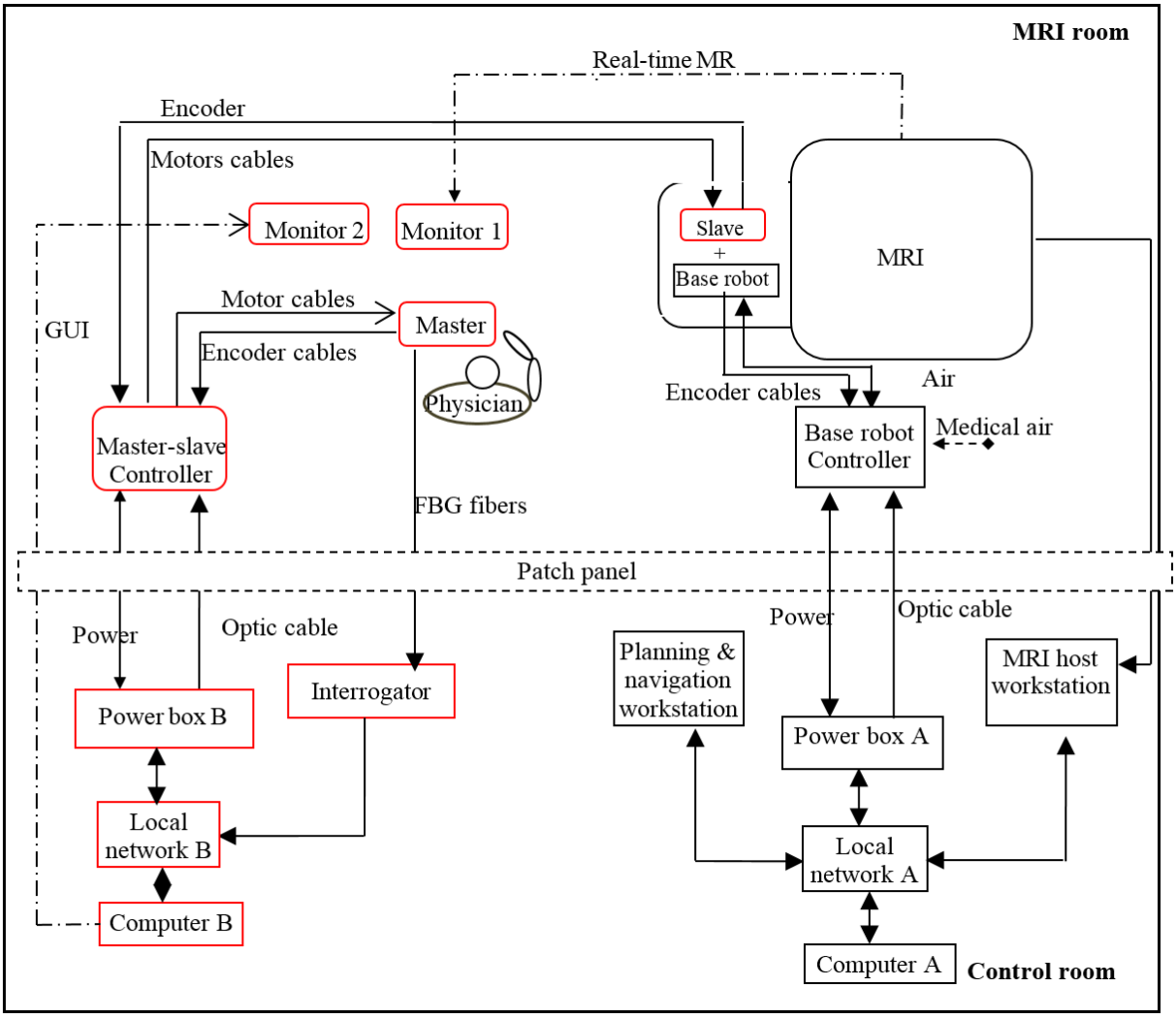

Fig. 1: Schematic of the entire system components: Right: base robot system components are shown in black boxes. Left: teleoperation needle steering system components developed in this study are shown in red boxes.

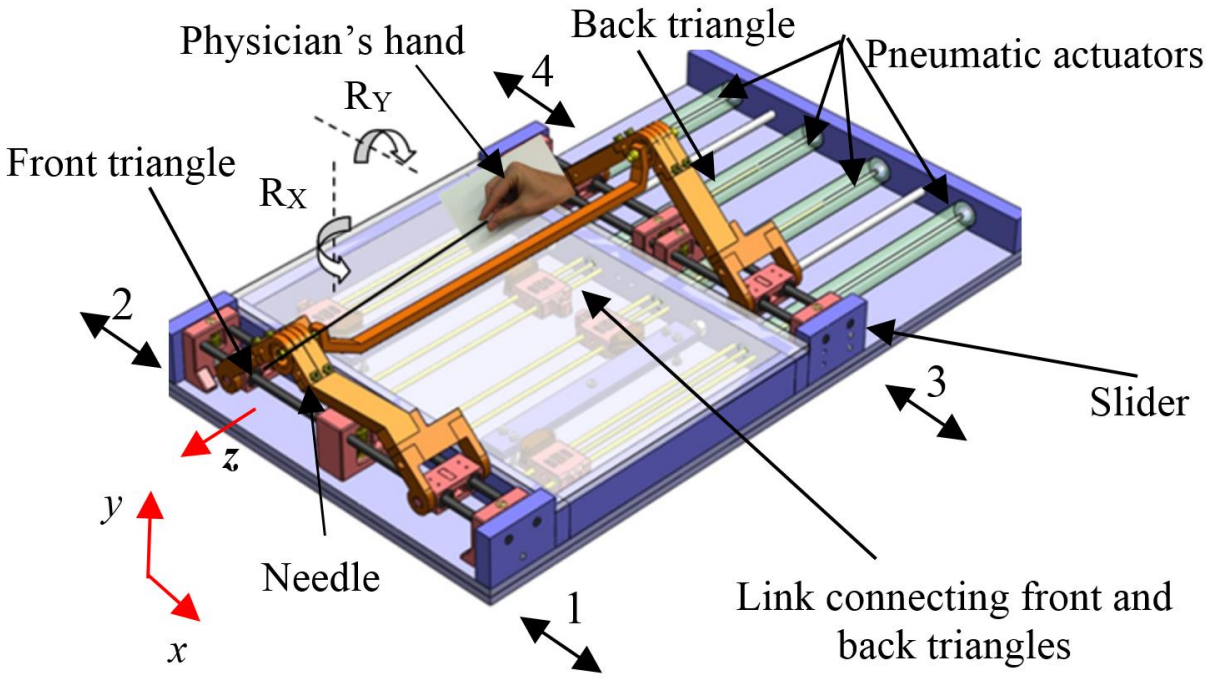

Fig. 2: Base robot is a 4-DOF pneumatic robot for transperineal needle placement into prostate under MRI-guidance. It provides translations in x, and y directions as well as angulations in Rx and Ry directions. Insertion is performed manually.

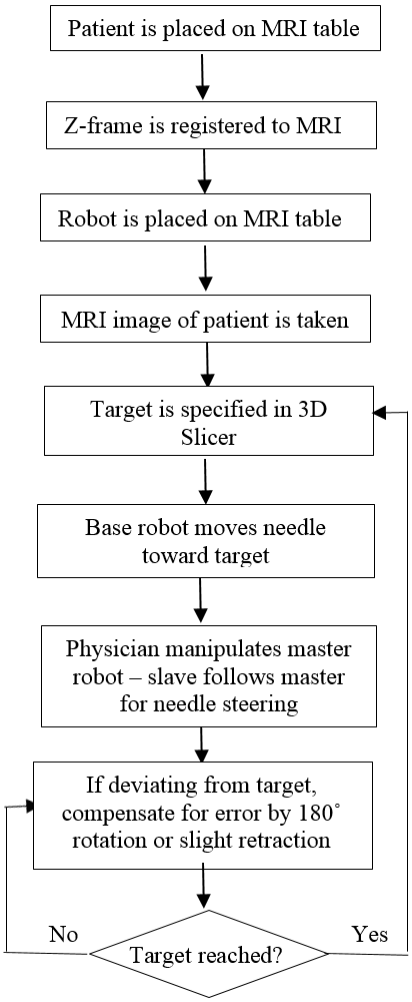

Fig. 3. A flowchart showing the procedure workflow using the postposed system.

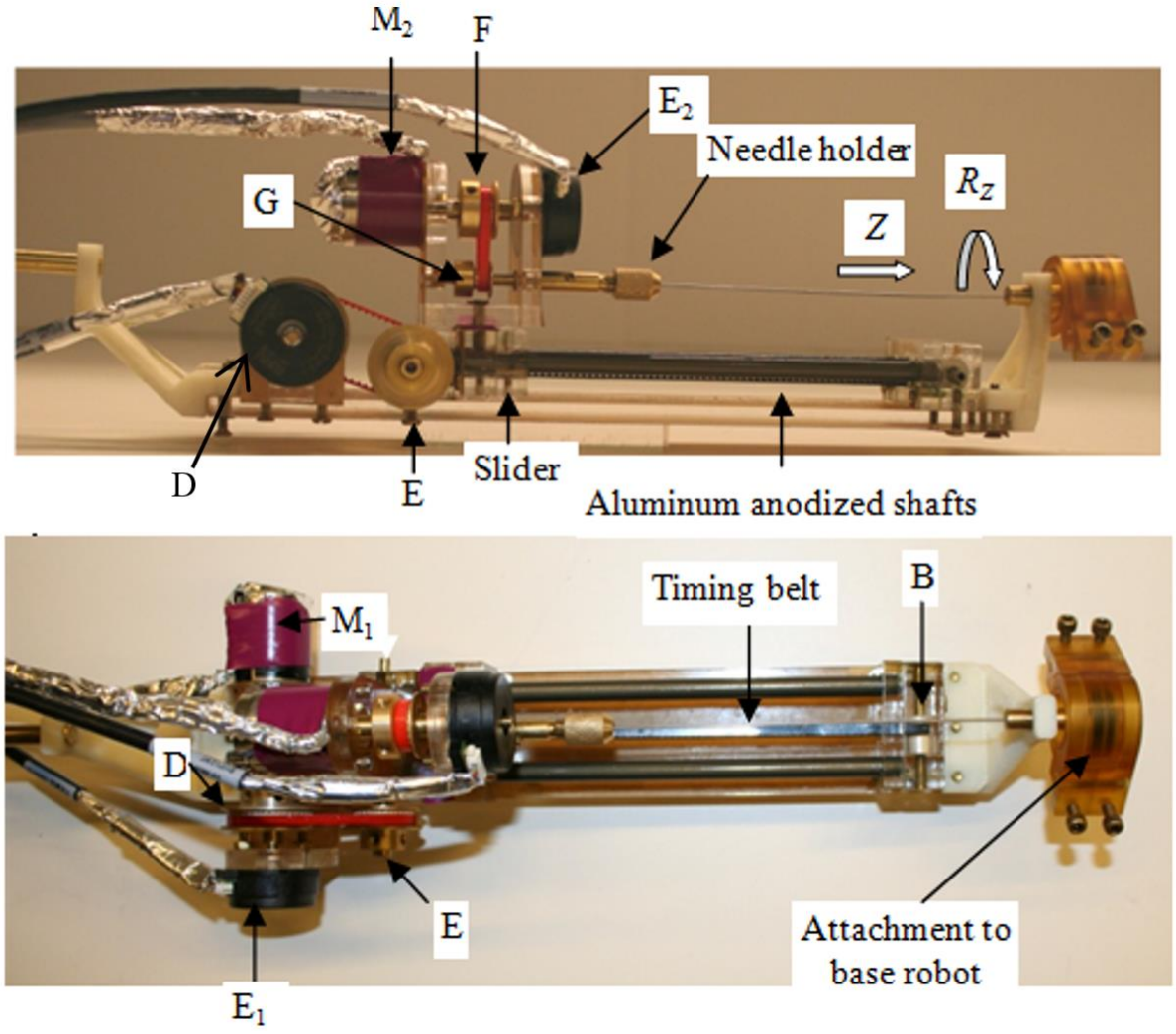

Fig. 4. MRI-compatible needle steering slave robot with 2-DOF: translation along Z (superior-inferior) and rotation of the bevel-tip needle RZ. Cables are shielded carefully.

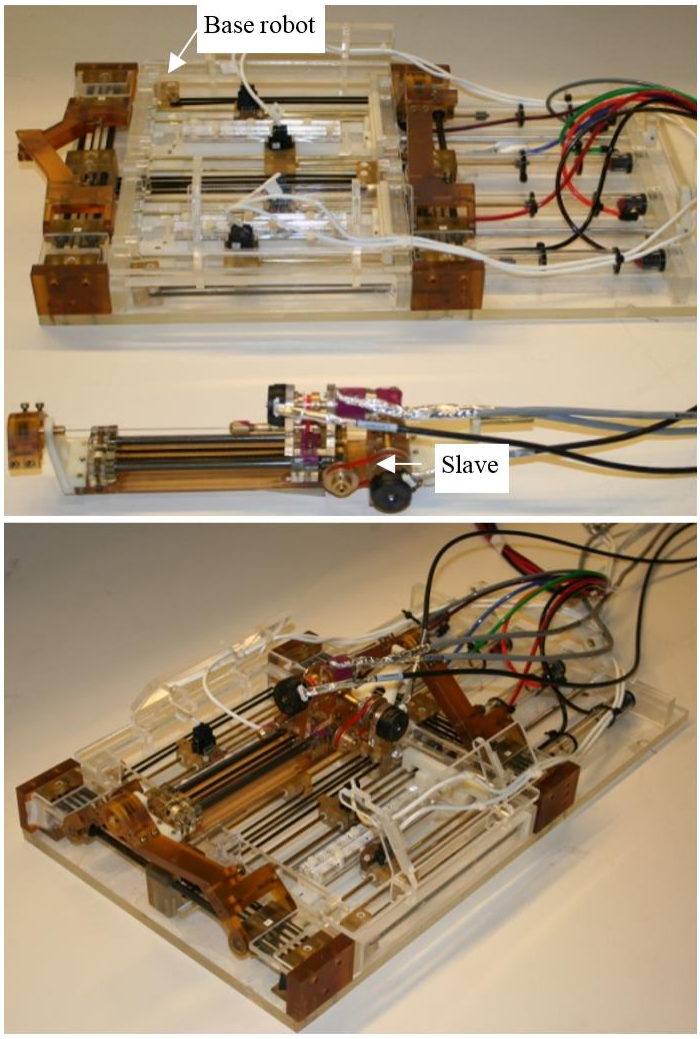

Fig. 5. Top: the slave can be easily attached to the base robot, Bottom: the needle steering module is integrated with the base robot. The base robot provides the macro needle positioning and the slave provides insertion and final adjustments (i.e. steering).

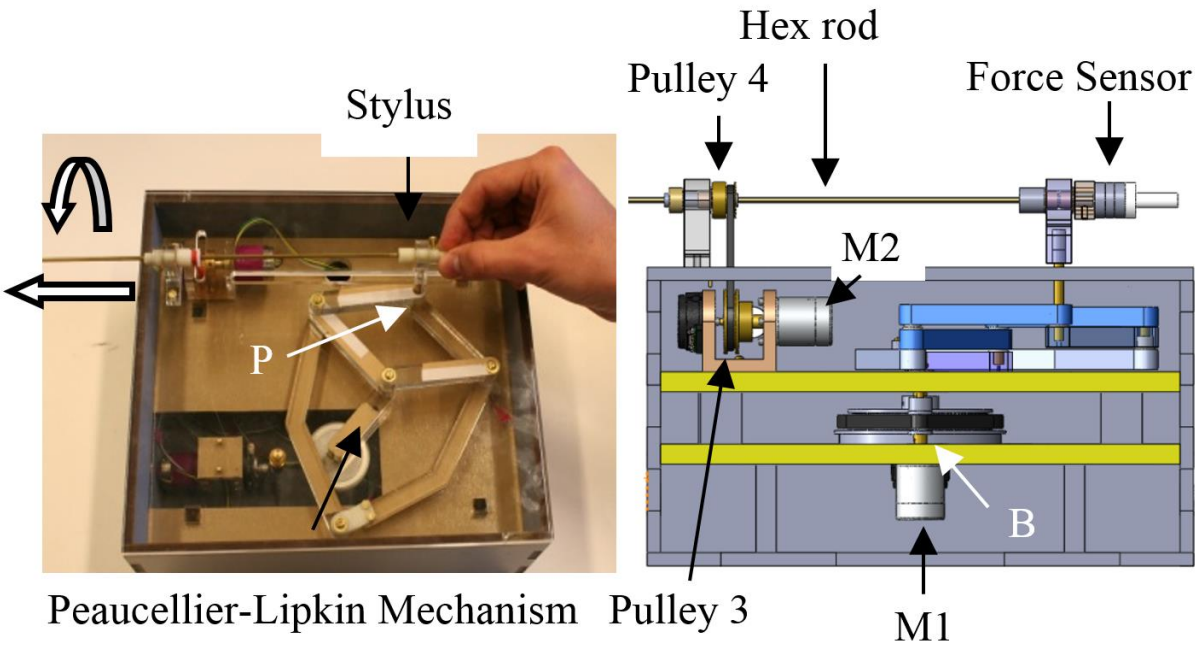

Fig. 6: Left: Prototype of the master robot in top view: Peaucellier-Lipkin mechanism was employed to convert rotary motion of motor to linear motion. Right: CAD presentation showing rotation module in front view: the power is transmitted with a timing belt. Both motors and both encoders are fixed to the base.

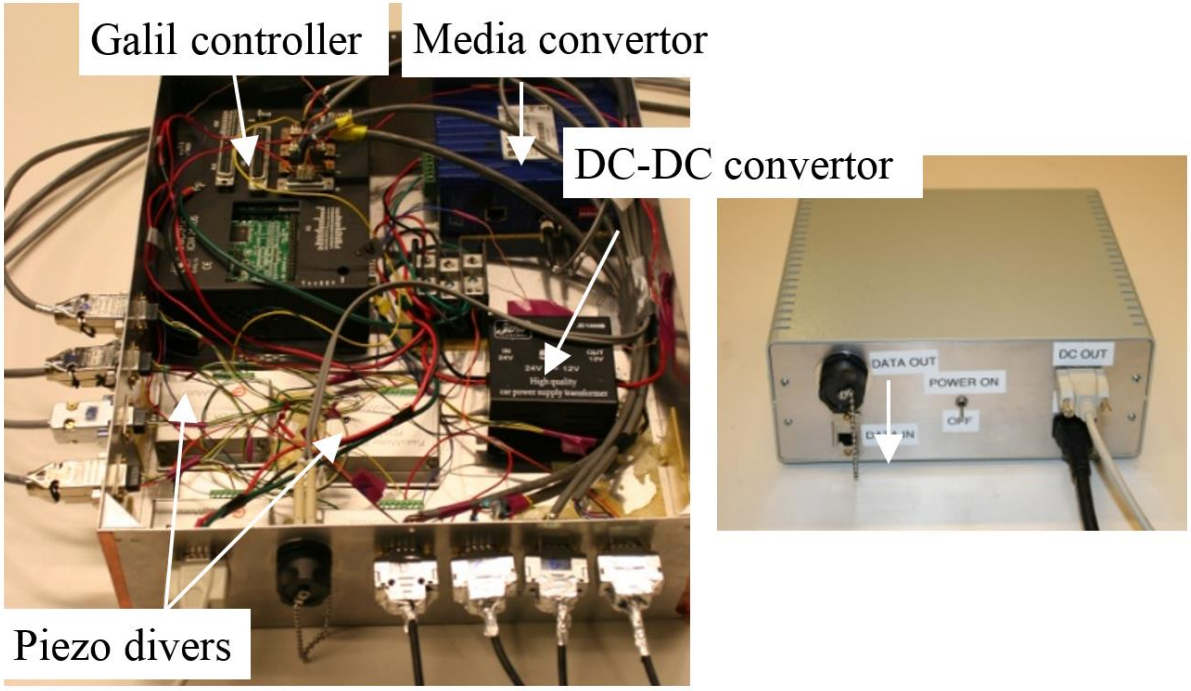

Fig. 7. Left: Master-slave controller box intside view, Right: Power supply box.

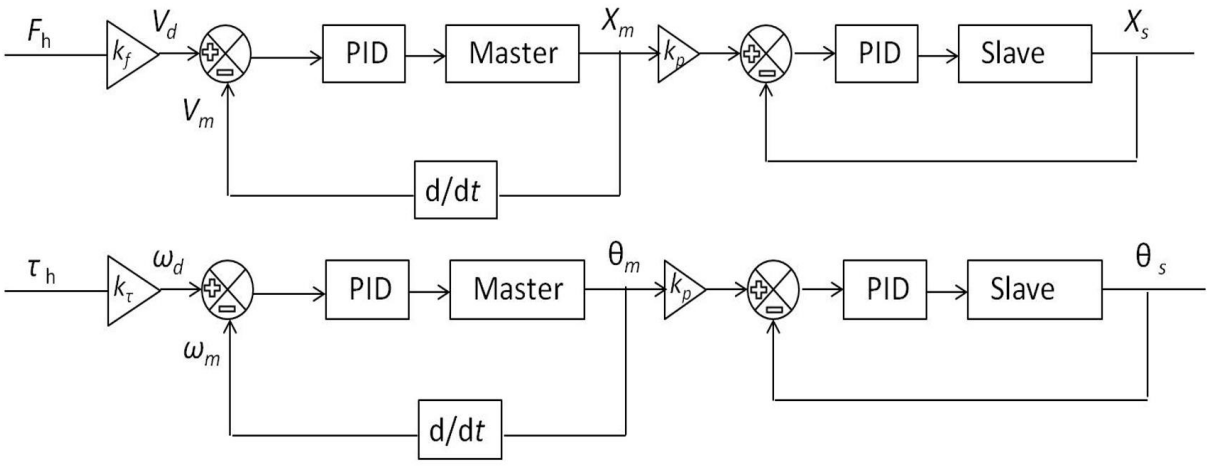

Fig. 8. Controller architecture for master-slave system: cooperative control for the master and position tracking for slave.

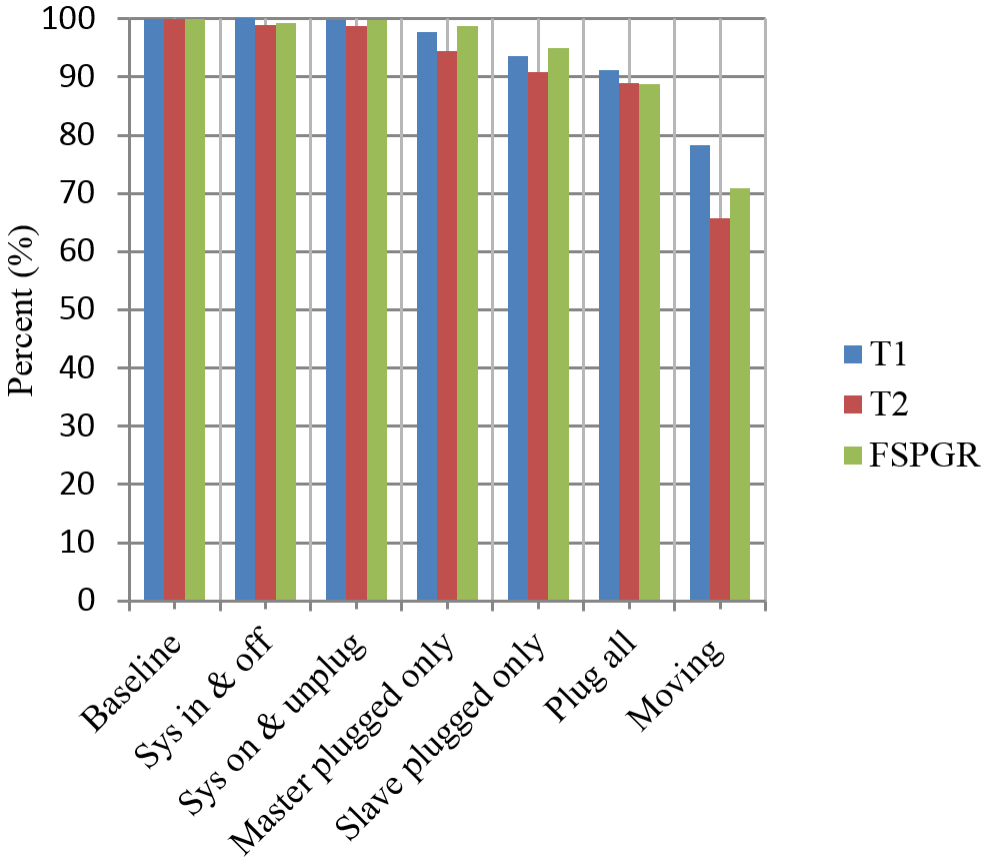

Fig. 9: SNR results.

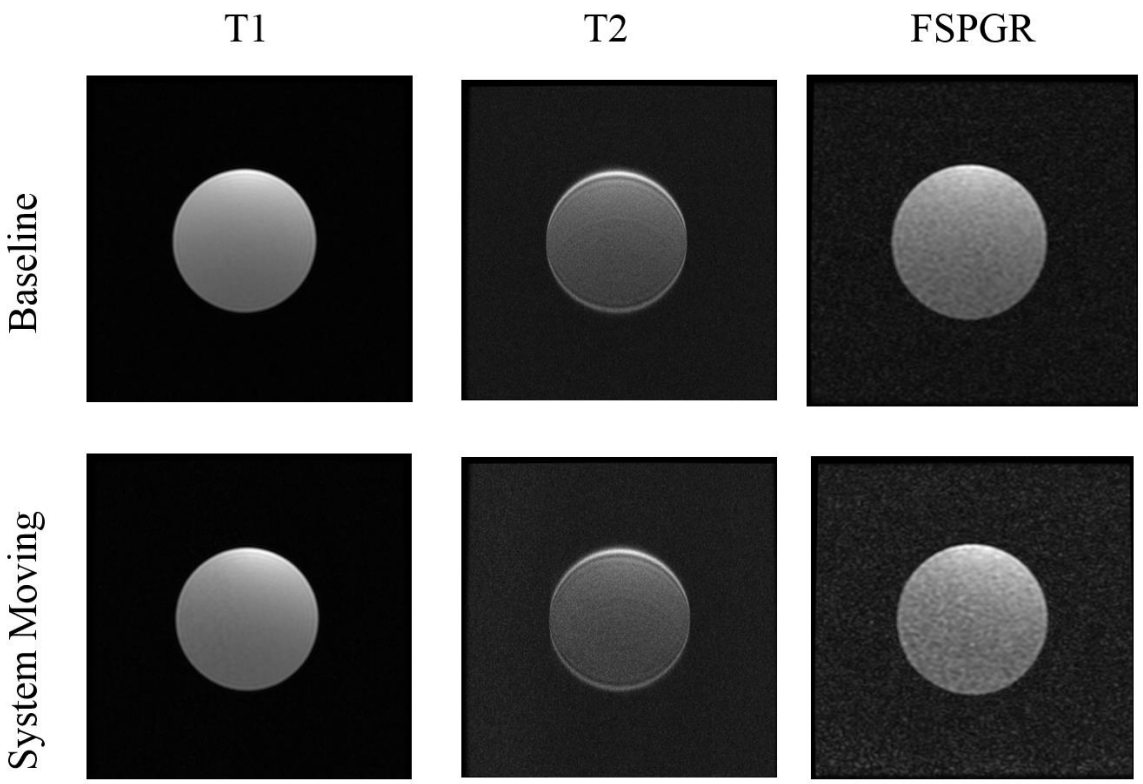

Fig. 10: Visual comparison of different imaging sequences for the baseline with the system moving; the difference is insignificant.

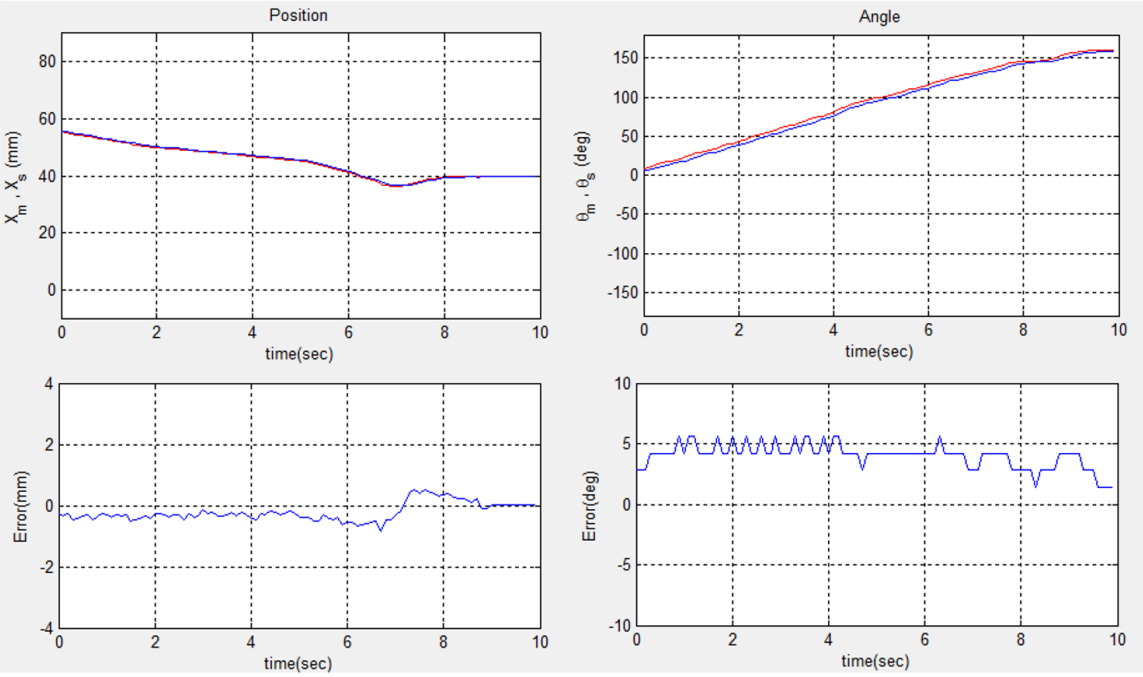

(a) (b)

Fig. 11: Position tracking when the needle is inserted into the phantom: (a) Translational motion, and (b) rotary motion. The steady state error is approaching zero in both cases.

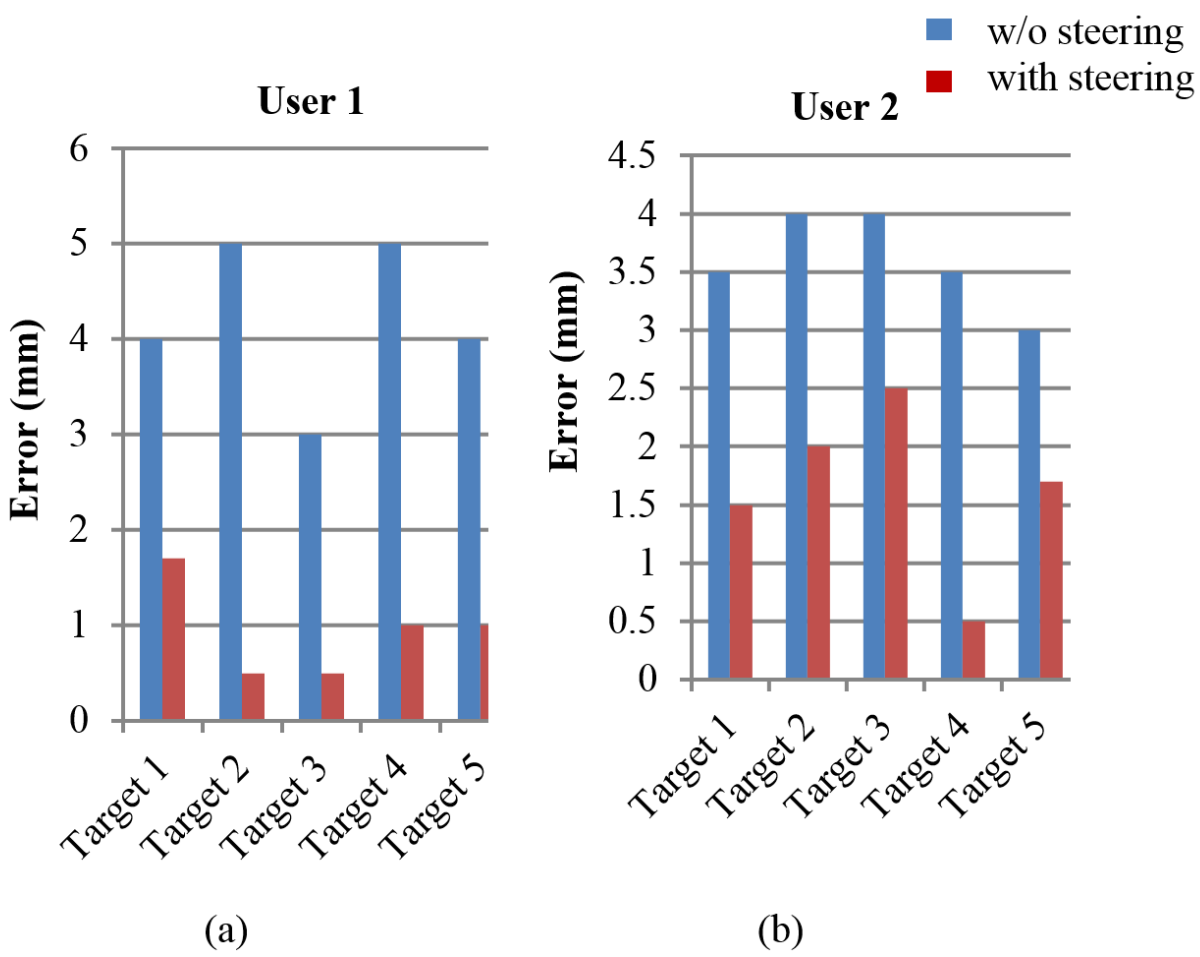

Fig. 12. The effectiveness of a simple steering method: the blue bars show the errors without steering and the red bars show the errors with steering. Steering means the needle was stopped half-way through, rotated 180 deg, and the insertion was continued until reaching the opposite side of the phantom. The average error was reduced from 4.2 mm to 0.9 mm for User 1 and from 3.6 mm to 1.6 mm for user 2.

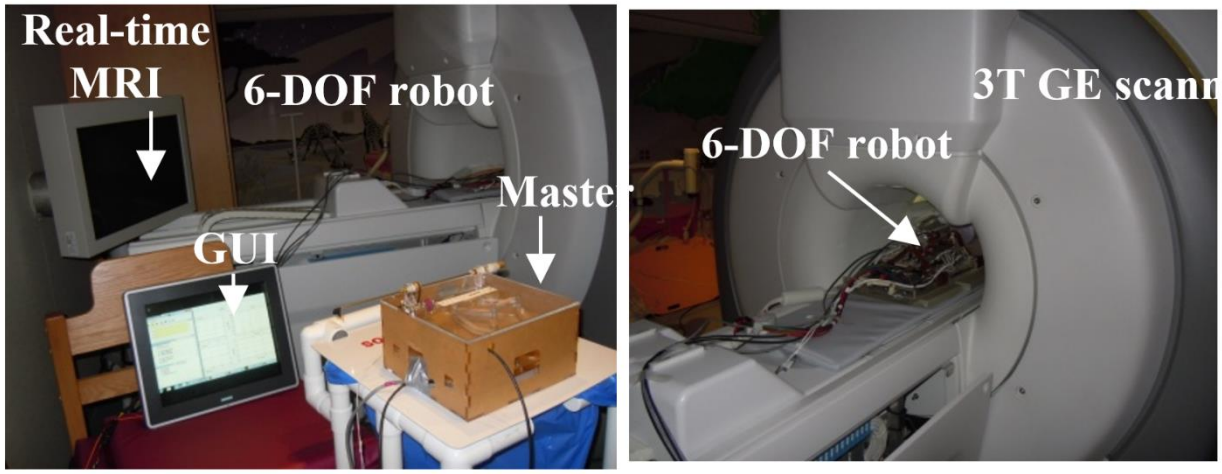

Fig. 13: Experiment setup for teleoperated needle steering under MRI guidance: (a) physician steers needle remotely using the master robot under continuous MRI, (b) real experimental setup with phantom, one monitor for continuous MRI and one for GUI, and (c) 6-DOF robot is placed inside the bore.

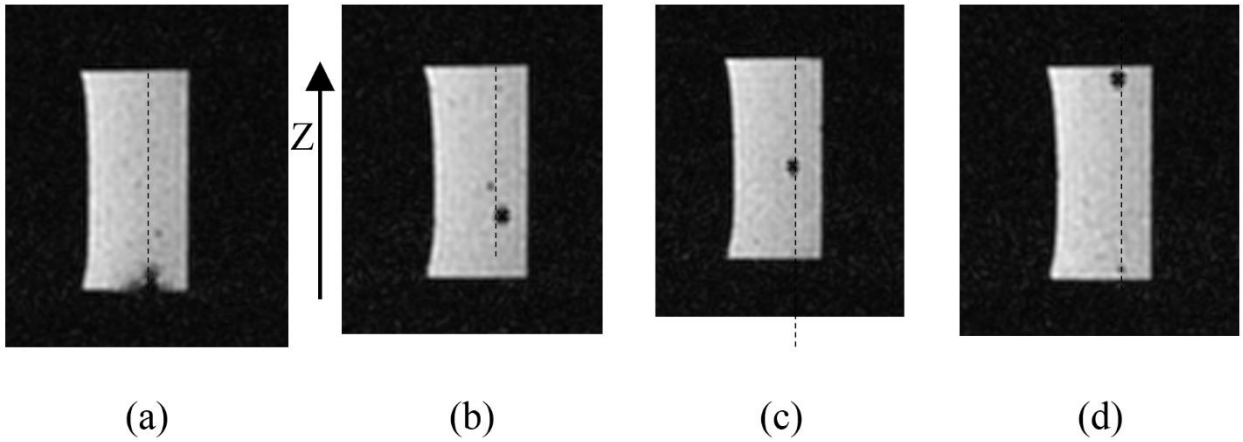

Fig. 14: Continuous MR image of the needle during insertion: needle is gradually inserted toward the other side of the phantom. The dark spot is the needle tip artifact. The needle tip artifact is depicted in 4 intervals during needle insertion. At time step (c), the operator rotates the needle 180 degree to steer the needle tip toward the opposite direction. The phantom is shown in sagittal plane.